Biological: Full–length

Structural analysis of hydroxyapatite coating on magnetite nanoparticles using energy filter imaging and electron tomography

Mitsuhiro Okuda[1,2], Masaki Takeguchi[2], Órla Ó Ruairc[3], Motohiro Tagaya[1], Yufang Zhu[4], Ayako Hashimoto[4], Nobutaka Hanagata[1], Wolfgang Schmitt[3] and Toshiyuki Ikoma[1]*

[1]Biomaterials Center, National Institute for Materials Science, 1-2-1 Sengen, Tsukuba, Ibaraki, 305-0047, Japan, [2]Advanced Nano-Characterization Center, National Institute for Materials Science, 3-13 Sakura, Tsukuba, Ibaraki, 305-0003, Japan, [3]School of Chemistry, Trinity College Dublin, Dublin 2, Ireland and [4]International Center for Young Scientists, National Institute for Materials Science, 1-2-1 Sengen, Tsukuba, Ibaraki, 305-0047, Japan
*To whom correspondence should be addressed. E-mail: IKOMA.Toshiyuki@nims.go.jp

Abstract   Magnetic nanoparticle (MNP) composites with a magnetite (Fe_3O_4) core and a hydroxyapatite (HAp, $Ca_{10}(PO_4)_6(OH)_2$) coating were prepared using a precipitation method and a subsequent hydrothermal treatment. The hydrothermal treatment diminished the lepidocrocite layer on the magnetite, enhanced the crystal growth of HAp and dissolved the MNPs. The divalent iron ions dissolved into solvent were not substituted for the HAp lattice. The three-dimensional (3D) nanostructure, the crystal morphology of HAp covered with the MNPs and the interfacial nanostructure of magnetite/HAp were analyzed using an energy-filter transmission electron microscopy (EF-TEM) and visualized by computer tomography in transmission electron microscopy (TEM). EF-TEM and 3D reconstruction images using a tilted series of high-angle annular dark-field images showed that the needlelike HAp nanocrystals covered with a magnetite core and the crystal growth of HAp attached to the magnetite surface was inhibited as a result of the lower density of the nucleation site of the lepidocrocite layer. The dissolution of iron ion from MNPs and the interfacial interaction of HAp and magnetite could cause the needlelike morphology of HAp nanocrystals.

Keywords   electron tomography, magnetite, hydroxyapatite, magnetic nanoparticle, hyperthermia, MRI

Received   27 August 2009, accepted 29 September 2009, online 6 November 2009

Introduction

Magnetic nanoparticles (MNPs) have attracted a great deal of attention in biomedical applications such as biomolecular separation, targeted drug delivery, a contrast agent for magnetic resonance imaging (MRI) and cancer diagnosis on hyperthermia [1]. In particular, magnetite (Fe_3O_4) and maghematite (γ-Fe_2O_3) have been widely investigated, as two of the most promising MNPs for biomedical materials because of their superior magnetic properties and biocompatibility with relatively low toxicity and high metabolic characteristics. Furthermore, a short T2 relaxation time and high-saturation magnetization make it possible to enhance the image contrast of MRI and the effectiveness of cancer diagnosis on hyperthermia.

Surface modification of the MNPs, for practical application, is indispensable to improve functions such as biomolecular recognition and stability in tissues and cells. Many researchers have explored the coating materials on MNPs by means of the introduction of functional groups, ligand–receptor reactions and with the improved structural stability and solubility in tissues, such as dextran [2], polyethylene glycol [3], silica [4], gold [5] and hydroxyapatite (HAp, $Ca_{10}(PO_4)_6(OH)_2$) [6,7]. HAp shows excellent biocompatibility and has been investigated as a drug delivery carrier [8]. Some researchers have already described 'Magnetite-HAp composites' using co-precipitation [6] and hydrothermal methods [7] and have examined their magnetic properties for hyperthermia applications. However, it has not been made clear whether the composites were mixture- or epitaxially grown on magnetite surfaces, which introduce a chemical binding among each other.

Recently, we described how crystalline HAp precipitates grow on magnetite nanoparticles through a biomimetic process—biomineralization; to mimic the tooth of chiton, HAp nanocrystals were formed through a lepidocrocite (γ-FeOOH) intermediate layer on a magnetite layer [9]. Thus, we produced a lepidocrocite layer on the surface of magnetite MNPs like chiton teeth and then formed the HAp using a layer-by-layer technique [10]. However, it was not clear whether HAp directly adhered to the magnetite surface to form the expected core/shell structure successfully. A detailed understanding of the nucleation process and the growth of HAp on magnetite MNPs is needed to optimize the condition of HAp coating.

High-resolution imaging, such as scanning electron microscopy (SEM), atomic force microscopy (AFM) and scanning tunnel microscopy (STM), are useful for the observation of micro- to nano-structures, for which techniques are limited in surface imaging and are unsuitable for characterizing the core/shell interface structure. Conventional transmission electron microscopy (TEM) is a powerful tool for imaging internal structures but cannot readily distinguish the three-dimensional (3D) features of the interfacial structure between core and shell materials. On the other hand, computer tomography (CT) in TEM (TEM-CT) has been developed, and thereby 3D analyses with a nanometer scale are avail-able in high resolution for the complex core/shell structures [11].

This paper aims at revealing the nano-level interfacial structure of a magnetite core and HAp coating using TEM-CT. The structures of magnetite/HAp MNP composites prepared by biomimetic mineralization are three-dimensionally reconstructed by TEM-CT, followed by an extraction of images sliced at specific sites with nanometer resolution. Combining with elemental imaging by energy-filtered transmission electron microscopy (EF-TEM), the interfacial structure of HAp adhesion on magnetite is elucidated, and the process of nucleation and growth of HAp on magnetite MNP are discussed.

Materials and methods

Sample preparation

A method proposed by Deng *et al.* was employed to fabricate a magnetite MNP [12]. $FeCl_3 \cdot 6H_2O$ (1.35 g, 5 mmol) was dissolved in ethylene glycol (40 mL), followed by the addition of sodium acetate (3.6 g) and polyethylene glycol (1.0 g). The mixture was stirred vigorously for 30 min and then sealed in a Teflon-lined stainless-steel autoclave (300 mL capacity). The autoclave was heated at 200°C for 8 h in an oven. After cooling to room temperature, the black products were washed several times with ethanol and dried at 60°C for 6 h and then dispersed in ethanol to form a 1 wt% magnetite suspension.

Magnetite/HAp MNP composites were prepared by a precipitation method and the subsequent hydrothermal method. Hundred milliliter of $K_2HPO_4 \cdot 3H_2O$ solution (24 mmol L^{-1}) was heated at 80°C, and the pH was controlled by means of a KOH solution (5 mol L^{-1}), and 1 mL of magnetite suspension was then added and stirred for 30 min. Hundred milliliter of $CaCl_2$ solution (40 mmol L^{-1}) was added at the rate of 25 mL min^{-1} into the high-alkaline magnetite suspension. The final solution at pH 9.0 was transferred into a Teflon-lined stainless steel autoclave (300 mL, capacity) and heated at 160°C for 24 h in an oven. This suspension had a Ca/P ratio of 1.67, which is equal to a stoichiometric ratio of HAp. After cooling to room temperature, the resultant suspension was centrifuged at 20 000 *g* (196 000 m s^{-2}) for 10 min. The collected products were washed

three times with distilled water and three times with ethanol by centrifuge.

For X-ray powder diffraction (XRD) analysis, magnetite/HAp MNP composites in water were dried in an oven at 60°C. The crystalline phase of the product was analyzed using an X-ray diffractometer (Rigaku Ultima III©) under CuKα radiation at 40 kV and 40 mA in the 2θ range of 10–75°.

For TEM and SEM observations, the sample in ethanol was sonicated for 10 min, and 5 μL of the suspension was dropped onto a carbon film on a Cu mesh grid. After drying the mesh in air, the grid was immersed in 3 mL of ethanol for 5 min to completely wash the organic substances and then dried again.

Morphological analyses

Surface morphologies of the magnetite nanoparticles and the magnetite/HAp MNP composites were observed with a field emission SEM (FE-SEM, JEOL 7000F) at an accelerating voltage of 30 kV.

Elemental mapping by EF-TEM was performed on a JEOL 3000F filed emission TEM equipped with a Gatan imaging filter (Model 863 GIF Tridiem©) and a 2 k × 2 k charge-coupled device (CCD) camera (Ultrascan©). EF-TEM images of calcium (L edge, 347 eV), oxygen (K edge, 535 eV) and iron (L edge, 710 eV) maps were obtained by the three-window method.

The tilt series acquisition of high-angle annular dark-field scanning TEM (HAADF-STEM) images was performed on a JEOL 2100F field emission TEM equipped with an ADF detector (EM-24560, JEOL) and a digital image acquisition system (Digiscan II©, GATAN). The sample grid was placed in a holder (EM-21311HTR, JEOL), and the tilt series of a magnetite/HAp MNP composite was recorded from +60° to −60° at 2° decrements, giving a total of 61 images. The inner and outer semi-angles of the ADF detector for HAADF-STEM imaging were 71 and 190 mrad, respectively. In HAADF-STEM imaging, a 800 × 800 nm² area was acquired at the size of 1024 × 1024 pixel² at an exposure time of 63 s/frame including a dwell time of 60 μs/pixel. Acquisition of the tilt series was performed by the 3D Tomography Software© (GATAN) with automatic functions of stage tracking assist and dynamic focusing. In-focusing on acquisition of tilt series was
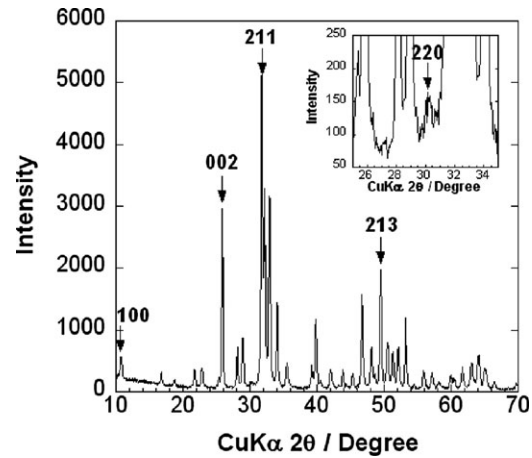
Fig. 1. XRD pattern of magnetite/HAp MNP composites treated with a hydrothermal treatment. Index of (100), (002), (211) and (213) in the figure indicates Miller's indices of HAp. The inset figure shows the expansion of the XRD pattern around (220) diffraction of magnetite. All diffraction peaks except (220) at 30.1° are attributed to HAp (JCPDS 09-0432).

adjusted manually. After extracting selected area tilt series (600 × 600 pixel² image) from row tilt series, an image alignment with band pass filter and 3D reconstruction using the simultaneous iterative reconstruction technique (SIRT) with 40 iterations were calculated by the 3D Tomography Software© (GATAN).

Results and discussion

Figure 1 shows the XRD pattern of magnetite/HAp MNP composites treated with hydrothermal treatment. These diffractions corresponded to HAp and magnetite. The typical diffractions of (100), (002), (211) and (213) attributed to the HAp phase and the maximum diffraction of (220) at 30.1° in 2θ degree attributed to the magnetite were detected, respectively. It should be noted that the diffractions in the lepidocrocite phase were indistinguishable. As we previously described [10], the magnetite/HAp MNP composites before the hydrothermal treatment showed a XRD diffraction of the lepidocrocite at 26° in 2θ degree, and a typical infrared (IR) adsorption peak attributed to the lepidocrocite at 758 cm⁻¹, suggesting that there was an intermediate layer between the magnetite and HAp [12]. The IR adsorption peak at 758 cm⁻¹ of the magnetite/HAp MNP composites after hydrothermal treatment was indistinguishable (data not shown). In the hydrothermal treatment, the lepidocrocite layer in the MNPs
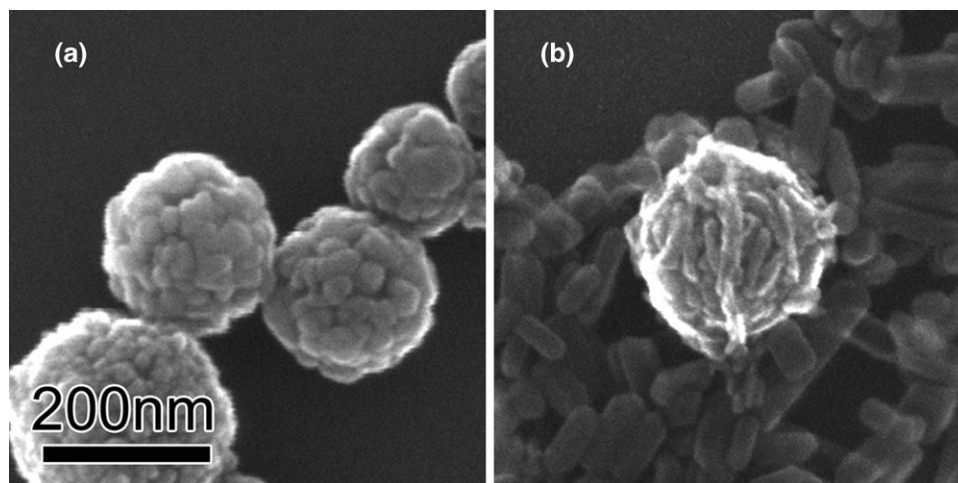
Fig. 2. FE-SEM images of (a) magnetite spherical MNPs and (b) a magnetite/HAp MNP composite that were covered by needlelike HAp nanocrystals.

composite did not appear because the hydrothermal treatment can transfer the hydrothermally unstable lepidocrocite to the magnetite. The amount of magnetite crystals apparently decreased during the hydrothermal process due to the dissolution of the magnetite in an alkaline solution. On the other hand, the crystallinity of HAp in the MNPs hydrothermally treated was higher than that of the HAp precipitation, indicating that HAp nanocrystals had been grown.

Figure 2 shows FE-SEM images of (a) magnetite MNPs and (b) magnetite/HAp MNP composites. The magnetite spherical MNPs as shown in Fig. 2a were constructed by an aggregation of cuboidal nanocrystals, 20–40 nm in size, with a spherical diameter of 100–250 nm. The spherical nanoparticles covered with needlelike crystals are shown in Fig. 2b, and larger platelike crystals were also observed around the spherical nanoparticles. While the platelike crystals measured 100–150 nm in length and 15–30 nm in width, the needlelike nanocrystals apparently were of a smaller size, measuring 70–90 nm in length and 5–15 nm in width. From the results of the XRD pattern, the platelike and needlelike nanocrystals were HAp, and the morphological differences could be attributed to the interaction of magnetite and HAp in the crystal growth. Thus, the interfacial structure of magnetite and HAp in the MNP was of importance to elucidate the mechanism of HAp crystal growth.

Figure 3 shows (a) TEM and EF-TEM images of a magnetite/HAp MNP composite and the elemental maps of (b) calcium, (c) oxygen, (d) iron, and (e) superimposed RB map of calcium and iron. There are three different morphologies with a gray contrast with needlelike nanocrystals aggregating around a centered spherical large particle with dark contrast and platelike nanocrystals. It should be noted that the needlelike nanocrystals cover the magnetite MNP surface, while the platelike nanocrystals are distributed around the spherical particle. Figure 3e is the superimposed image of Fig. 3b and d. It is clear that the spherical large particle is composed of iron and oxygen. On the other hand, the platelike and needlelike crystals contained calcium and oxygen, and the electron energy loss spectra of the platelike and needlelike crystals confirmed the presence of phosphorus. Combining with the results of the XRD pattern, it was identified that the spherical large particle is crystalline magnetite, and both the platelike and needlelike crystals are HAp. The iron exists only in the magnetite spherical MNPs, as shown in Fig. 3e, suggesting that the substitution of iron dissolved in the solvent in the apatite lattice could not occur during the hydrothermal treatment.

Figure 4 shows (a) HAADF-STEM image at a tilting angle of $0°$ and the sliced HAADF-STEM images of (b) xz and (c and d) xy directions extracted from the 3D reconstructed volume of the magnetite/HAp MNP composite. HAADF-STEM generally provides the minimization of unfavorable diffraction contrast and the atomic number (Z)-dependent high contrast image, the high contrast of which in a tilt series offers a tremendous advantage to 3D tomography reconstruction [11]. The Z-contrast of a
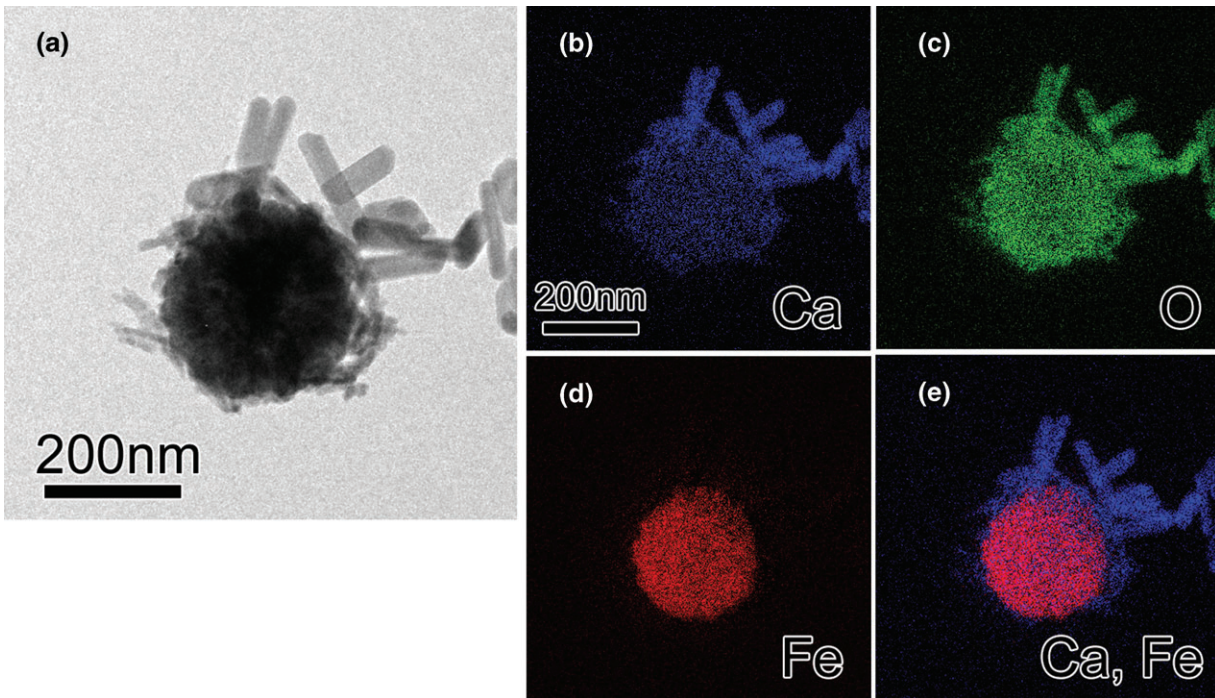
Fig. 3. TEM and EF-TEM images of a magnetite/HAp MNP composite. (a) TEM image, (b) calcium, (c) oxygen, (d) iron and (e) RB map (calcium, blue; and iron, red) maps. The elemental distributions were obtained by the three-window method. Calcium element distribution around the iron-containing particle is clearly observed.

heavy element such as iron shows a bright image. In this study, the sliced images extracted from the 3D reconstructed volume, as shown in Fig. 4b–d, clearly indicate that the internal nanopores in the magnetite spherical nanoparticle and the dimension of magnetite nanocrystals aggregated at 10–20 nm in size.

The sliced images at specific directions of longitudinal and header planes of nanocrystals are also available for length measurement. The platelike nanocrystals had 106.9 ± 33.4 nm and 37.8 ± 5.3 nm with an aspect ratio of 2.8, and the needlelike nanocrystals had 84.8 ± 26.1 nm and 8.6 ± 1.6 nm with an aspect ratio of 9.9. The hydrothermal treatment promotes HAp crystal growth as the platelike morphology; interestingly, the HAp covered with the magnetite spherical MNPs showed a different morphology with smaller needlelike crystals of HAp. The inhibition of HAp crystal was attributed to the dissolved divalent iron ions [13].

Obviously, the needlelike HAp nanocrystals shown in Fig. 4c and d were not evenly covered, with the surfaces of the magnetite spherical nanoparticles in random directions, but HAp crystal growth was initiated on the magnetite surface with tip or side at-

tachments. It is known that the lepidocrocite intermediate layer on magnetite spherical MNPs plays an important role as a nucleation site for HAp growth. In our previous report [10], there was a lepidocrocite layer detectable by XRD and IR in the magnetite/HAp MNP composites prepared using a precipitation method. The hydrothermal treatment reduced the lepidocrocite layer undetectable by XRD and TEM-CT, and thus HAp coverage was limited due to the lower density of the nucleation sites. Both dissolution of iron ions from magnetite spherical MNPs and the interfacial interaction of HAp and magnetite could strongly affect the crystal growth of HAp.

Concluding remarks

MNP composites with a magnetite core and a HAp coating were successfully prepared using the precipitation method and subsequent hydrothermal treatment. The results of EF-TEM and the 3D reconstructed TEM-CT images showed that the magnetite/HAp MNP composites were composed only of needlelike HAp nanocrystals covering the magnetite spherical MNPs that had internal nanopores. The crystal growth of needlelike HAp nanocrystals was restricted due to the effects of the dissolved divalent
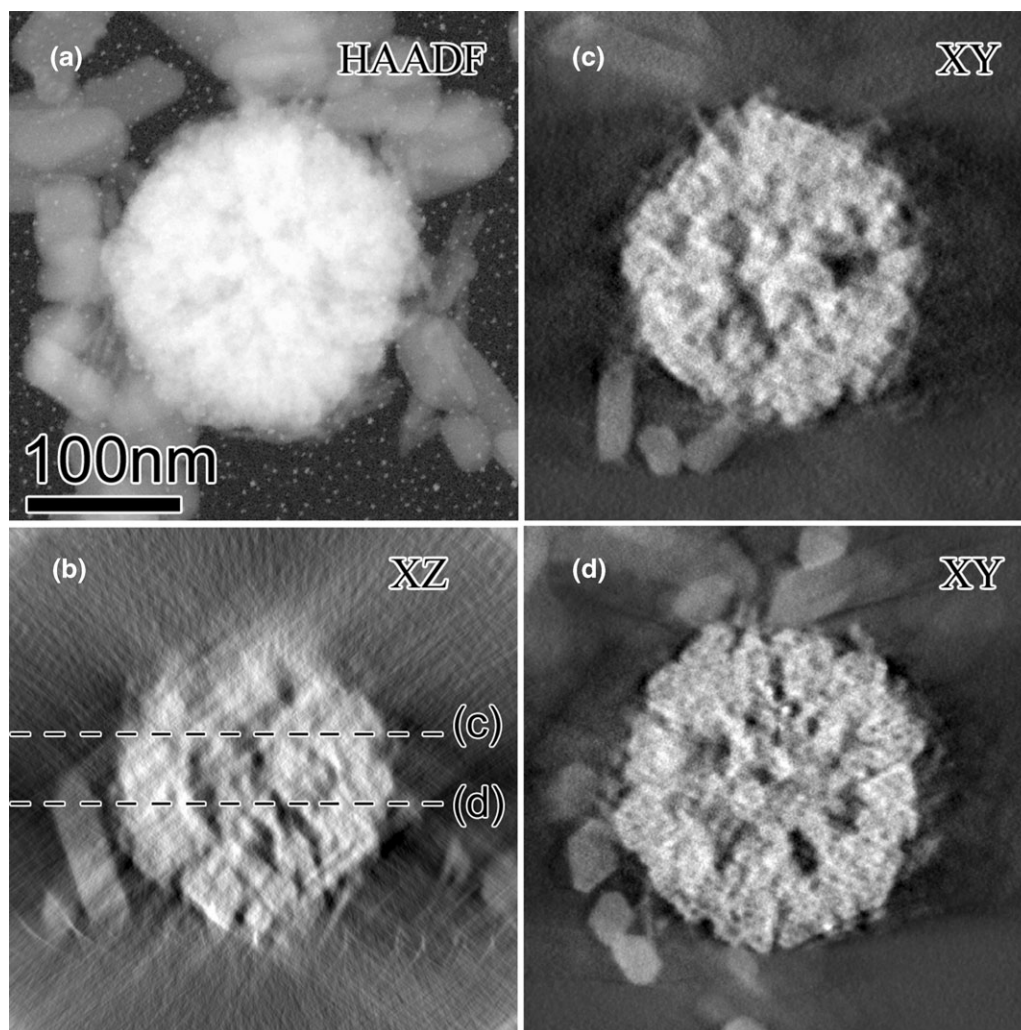
Fig. 4. HAADF-STEM images extracted from 3D reconstruction by TEM-CT of a Fe_3O_4 core and HAp coating. (a) HAADF-STEM image, (b) xz sliced image including the sliced depth of xy images as dashed lines, and (c and d) xy sliced images at different depths. Supplementary information shows the movie of xy sliced images.

iron as well as the interfacial interaction of HAp and magnetite. The coverage of HAp on the magnetite surface was limited due to the lower density of nucleation sites of lepidocrocite for HAp nanocrystals.

Supplementary data

Supplementary data are available at http://jmicro. oxfordjournals.org/.

References

1 Mornet S, Vasseur S, Grasset F, and Duguet E (2004) Magnetic nanoparticle design for medical diagnosis and therapy. *J. Mater. Chem.* **14**: 2161–2175.

2 Berry C C, Wells S, Charles S, and Curtis A S G (2003) Dextran and albumin derivatised iron oxide nanoparticles: influence on fibroblasts *in vitro. Biomaterials* **24**: 4551–4557.

3 Inada Y, Ohwada K, Yoshimoto T, Kojima S, Takahashi K, Kodera Y, Matsushima A, and Saito Y (1987) Fibrinolysis by urokinase endowed with magnetic property. *Biochem. Biophys. Res. Commun.* **148**: 392–396.

4 Tartaj P, Gonzµlez-Carreæo T, and Serna C J (2001) Single-step nano-engineering of silica coated maghemite hollow spheres with tunable magnetic properties. *Adv. Mater.* **13**: 1620–1624.

5 Chen M, Yamamuro S, Farrell D, and Majetich S A (2003) Biological applications: particles and sensors. *J. Appl. Phys.* **93**: 7551–7553.

6 Wu H C, Wang T W, Sun J S, Wang W H, and Lin F H (2007) A novel biomagnetic nanoparticle based on hydroxyapatite. *Nanotechnology* **18**: 165601

7 Murakami S, Hosono T, Jeyadevan B, Kamitakahara M, and Ioku K (2008) Hydrothermal synthesis of magnetite/hydroxyapatite composite material for hyperthermia therapy for bone cancer. *J. Ceram. Soc. Japan.* **116**: 950–954.

8 Ikoma T, Tonegawa R, Watanabe H, Chen G P, Tanaka J, and Mizushima Y J (2007) Drug-supported microparticle of calcium carbonate nanocrystals and its covering with hydroxyapatite *J. Nanosci. Nanotechnol.* **7**: 822–827

 9 Wealthall R J, Brooker L R, Macey D J, and Griffin B J (2005) Fine structure of the mineralized teeth of the chiton *Acanthopleura echinata* (Mollusca: polyplacophora). *J. Morphol.* **265**: 165–175.

10 Ó Ruairc Ó, Tonegawa T, Tagaya M, Okuda M, Takeguchi M, Zhu Y, Hanagata H, Schmitt W, Ikoma T (2009) Biomimetic approach to lepidocrocite-mediated magnetite-hydroxyapatite nanocomposites materials letter. Submitted.

11 Midgly P A, and Weyland M (2003) 3D electron microscopy in the physical sciences: the development of Z-contrast and EFTEM tomography. *Ultramicoscopy* **96**: 413–431.

12 Deng H, Li X, Peng Q, Wang X, Chen J, and Li Y (2005) Monodisperse magnetic single-crystal ferrite microspheres. *Angew. Chem. Int. Ed.* **44**: 2782–2785.

13 Morrissey R, Rodriguez-Lorenzo L M, and Gross K A (2005) Influence of ferrous iron incorporation on the structure of hydroxyapatite. *J. Mater. Sci. Mater. Med.* **16**: 387–392.